

Hydrodynamic instabilities provide a generic route to spontaneous biomimetic oscillations in active filaments

Abhrajit Laskar,¹ Rajeev Singh,¹ Somdeb Ghose,¹ Gayathri Jayaraman,¹ P. B. Sunil Kumar,² and R. Adhikari¹

¹The Institute of Mathematical Sciences, CIT Campus, Chennai 600113, India

²Department of Physics, Indian Institute of Technology Madras, Chennai 600036, India

(Dated: July 5, 2022)

Microscopic living organisms locomote in viscous fluids through spontaneous beating of filamentous structures anchored at one end, such as flagella and cilia. Prokaryotic flagella rotate rigidly like a corkscrew, while eukaryotic flagella are flexible and oscillate in a plane. We observe similar biomimetic beating behavior *in silico* by clamping an active filament at one end and solving for hydrodynamics interactions. Highly active filaments become unstable to transverse perturbations and exhibit autonomous oscillations. This transition into a limit cycle occurs via a supercritical Hopf bifurcation. The time period and amplitude of beating increase with increasing filament length, but collapse to a master curve on appropriate scaling. An analytical calculation of the spectrum of the filament model in the free-draining approximation fails to capture oscillatory behavior, emphasizing the crucial role played by hydrodynamic interactions.

Nonequilibrium processes by which biochemical energy is converted to mechanical stress are essential for life. These processes enable the autonomous motility of living organisms which, otherwise, would be impossible in equilibrium. At the microscale the engines of motility are primarily cilia and flagella, which are bundles of inextensible elastic filaments that oscillate when forced by the energy transduction of molecular motors. Although the mechanism behind this behavior has been studied in varying degrees of detail over the years [1–12], the contribution of hydrodynamic interactions (HI) has generally been overlooked. The role played by HI in biomimetic oscillations in synthetic active filaments has been studied in recent experiments [13, 14]. Motivated by these biological and biomimetic examples we seek to theoretically understand the contribution of HI to autonomous motion in active filaments. Here, we show that the competition between the destabilising effect of nonequilibrium hydrodynamic flow and the stabilising effect of bending and stretching elasticity provides a generic route to spontaneous biomimetic beating in a minimal model of active filaments [15]. Our results show that HI due to force-free and torque-free hydrodynamic flows generated by active energy transduction is sufficient to induce and sustain spontaneous oscillations in an inextensible filament. This minimal physical requirement then implies that biomimetic beating, previously observed only in bundles of active filaments (BAMs) [13, 14], can be replicated in a single filament, for instance, a chain of autocatalytic nanorods [16–19] or other synthetic active particles. Our results will help answer scientific questions like what minimal physical ingredients are required to generate synchronised metachronal waves, help guide the rational technological design of nanoscale machines like carpets of beating filaments that enhance fluid mixing, and bring us closer to uncovering the nonequilibrium mechanisms that drive biological motility.

Prokaryotic bacteria [20] as well as eukaryotic sperm cells [21, 22] employ rhythmic flagellar beating for loco-

motion in viscous fluids. Bacterial flagella rotate rigidly in corkscrew fashion [23, 24], whereas spermatid flagella behave more like flexible oars [25] with their beating mostly confined to a plane [26, 27]. Oscillatory motility in clamped flagella often arise spontaneously and, with an unlimited supply of energy, can persist indefinitely without any external or internal regulatory *pacemaker* mechanism [22, 28]. Autonomous motility as well as spontaneous beating due to hydrodynamic instabilities has been recently reproduced *in vitro* [13, 14], where a biomimetic active motor-microtubule assemblage has been shown to exhibit remarkable cilialike beating motion with hydrodynamic interactions playing a crucial role in synchronized oscillations [13].

In this Letter, we study a minimal active filament model [15] which, once clamped at one end, exhibits a variety of spontaneous beating phenomena in a three dimensional fluid. Our model filament consists of active monomeric beads in a viscous fluid connected through spring potentials that enforce inextensibility, semiflexibility and self-avoidance. Activity is modelled through force-free and torque-free singularities [29–34], since the *net* force and torque exerted on the fluid by any internally active system must vanish. The most dominant of these, the stresslet, is retained in our study. Hydrodynamic interactions are propagated by the appropriate Green’s functions. The equation of motion for the active filament [15] incorporating the effects of nonlinear elastic deformations, active processes and hydrodynamic interactions is

$$\dot{\mathbf{r}}_n = \sum_{m=1}^N [\mathbf{O}(\mathbf{r}_n - \mathbf{r}_m) \cdot \mathbf{f}_m + \mathbf{D}(\mathbf{r}_n - \mathbf{r}_m) \cdot \boldsymbol{\sigma}_m] \quad (1)$$

where \mathbf{r}_n is the location of the n -th bead, \mathbf{f}_n is the total elastic force on the n -th bead, and $\boldsymbol{\sigma}_n = \sigma_0(\mathbf{t}_n\mathbf{t}_n - \mathbb{I}/3)$ is stresslet tensor directed along the the local unit tangent \mathbf{t}_n . Here σ_0 sets the scale of the activity. The monopolar Oseen tensor \mathbf{O} and the dipolar stresslet tensor \mathbf{D} respectively propagate the elastic and active contributions

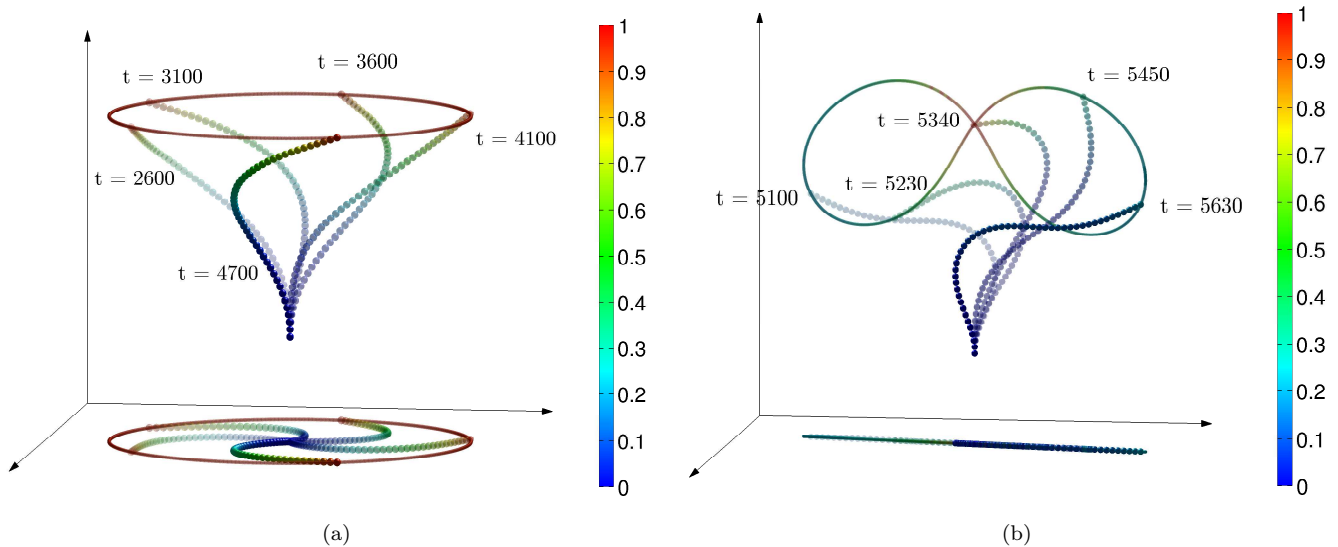


FIG. 1. (Color) Biomimetic oscillations of the clamped filament plotted at different times over an oscillation period T . In (a) we see rigid aplanar corkscrew rotation for $\mathcal{A} = 100$ while in (b) we see flexible planar beating for $\mathcal{A} = 200$. The color of the beads as well as the trace of the tip correspond to individual instantaneous monomer speeds.

to the flow. We impose clamped boundary conditions at one end and solve the equation of motion through direct summation of the hydrodynamic Green's functions. For a filament of length L and bending modulus κ the dynamics is characterised by the dimensionless measure of activity $\mathcal{A} = L\sigma_0/\kappa$, called the activity number [15].

Here we show, using linear stability analysis and numerical simulations, that the active filament has a hydrodynamic instability with increasing activity number. The containment of this linear hydrodynamic instability by the non-linear elasticity leads to spontaneously oscillating states. We briefly recall the mechanism of this linear instability [15]. Extensile activity produces flows that point outward in the longitudinal direction and inward in the normal direction. A spontaneous transverse perturbation breaks flow symmetry about the filament midpoint, resulting in a net flow along the outward filament normal. At low \mathcal{A} , this is countered by the elastic restoring force. Beyond a critical activity number \mathcal{A}_{c1} , linear elasticity is unable to balance the outward flow leading to a linear instability. The instability produces large filament deformations which are ultimately contained by the non-linear elasticity. Constrained by the clamp, the filament acquires a rigid corkscrew conformation and rotates about the initial axis. This rotational corkscrew motion is reminiscent of prokaryotic flagellar beating [23, 24]. We show this motion in Fig. 1(a) over one time period of oscillation together with the projection of the filament on the plane of the clamp. A section of the three-dimensional flow in a plane perpendicular to the plane of the clamp is shown in Figs. 2(a) and 2(b). The net flow points in the direction opposite to the filament curvature and the entire flow pattern co-rotates

with the filament.

With increasing \mathcal{A} the filament acquires greater flexibility. At a second critical value of the activity \mathcal{A}_{c2} , the filament motion collapses to a two-dimensional plane perpendicular to the plane of the clamp in which it beats spontaneously. This symmetric beating motion is reminiscent of eukaryotic flagellar beating [22, 26–28]. We show this motion in Fig. 1(b) over one time period of oscillation together with the projection of the filament on the plane of the clamp. The projection is now a line, showing that motion is confined to a plane. A section of the three-dimensional flow in the plane of beating is shown in Figs. 2(c) and 2(d). Two distinct types of filament conformations of opposite symmetry are now observed. In the *even* conformation shown in Fig. 2(c), the flow points in the direction opposite to the curvature as in the corkscrew state. However, in the *odd* conformation shown in Figs. 2(d), the flow has a center of vorticity at the point of inflection of the filament. This center of vorticity moves up the filament and is shed at the tip at the end of every half cycle.

In Fig. 3(a) we show the variation of the time period of oscillation T for both the corkscrew rotating and planar beating states for a filament of fixed length L . While the period T depends jointly on κ and σ_0 , a collapse is obtained when the period is scaled by the active relaxation rate $\Gamma_\sigma = \sigma_0/\eta L^3$, where η is the viscosity of the fluid. The oscillations become more rapid with increasing activity. In Fig. 3(b) we show the variation of the real parts of the two largest eigenvalue pairs obtained from a linear stability analysis. Here too, the data collapses when scaled by the active relaxation time Γ_σ^{-1} . All eigenvalues are real and negative as \mathcal{A} is increased from zero.

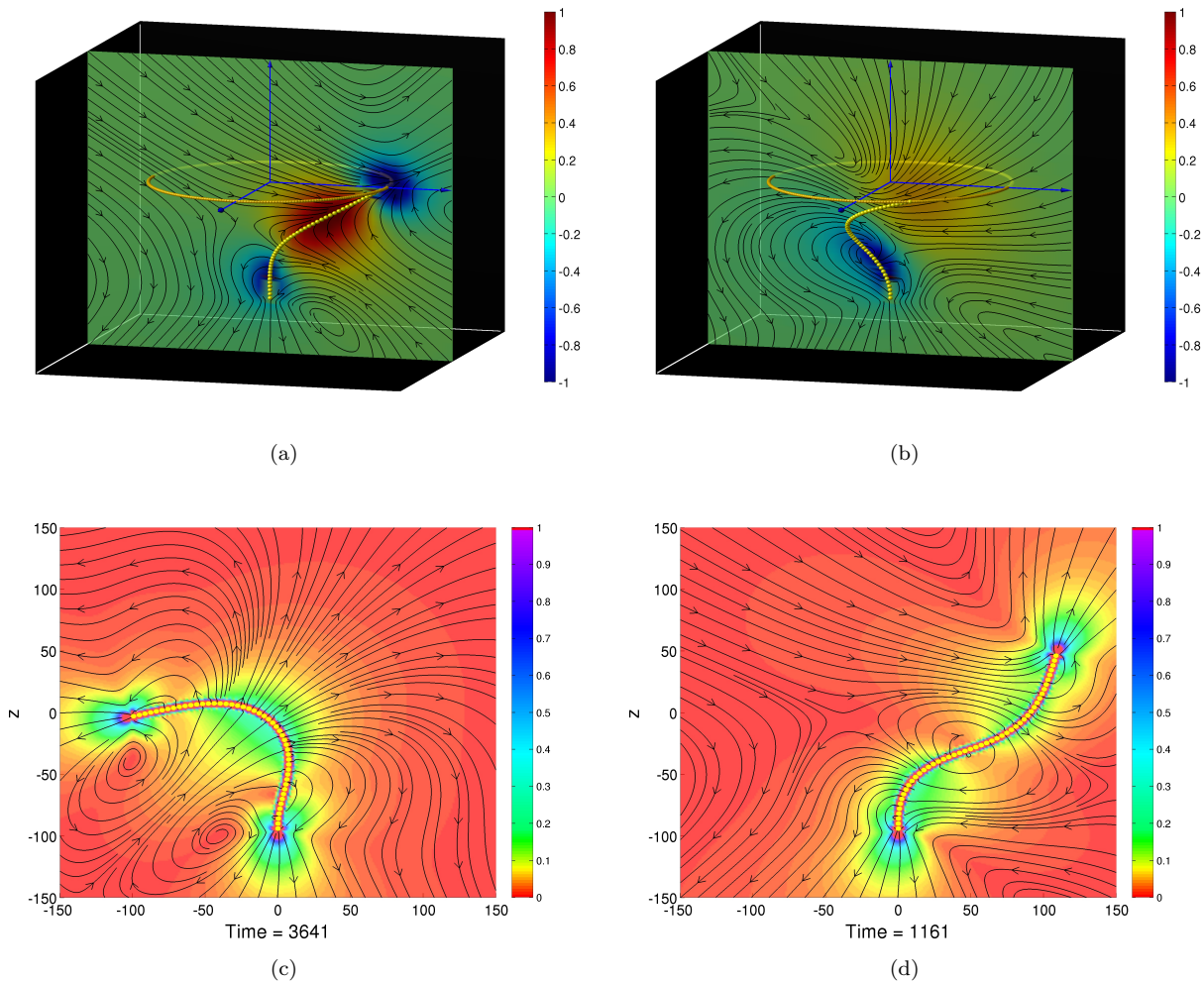


FIG. 2. (Color) Flow fields of (a, b) rigid aplanar corkscrew rotation and (c, d) flexible planar beating at two instants of the oscillation cycle. The color indicates the magnitude of the velocity field.

With increasing \mathcal{A} , the two largest eigenvalue pairs approach, converge, and become complex conjugate pairs. This corresponds to a transition from a stable node to a stable focus where the response changes from being overdamped to underdamped. With further increase of \mathcal{A} the complex eigenvalues approach the imaginary axis monotonically, crossing them at a critical value \mathcal{A}_{c1} . Through this supercritical Hopf bifurcation, the stable focus flows into the limit cycle corresponding to the corkscrew rotation. The variation of the real parts of the first eigenvalue pair reveals a striking feature of this filament. Since extensile activity produces flows that enhance the perturbation, the real parts for the most part increase with \mathcal{A} , according to expectation [11]. However, for a small but significant range of values of \mathcal{A} , we find that this quantity *decreases* with activity. Thus, in this window, extensile activity suppresses perturbations, which thus relax faster. With further increase of \mathcal{A} beyond \mathcal{A}_{c2} the corkscrew limit cycle transforms into the limit cycle cor-

responding to the planar beating state. Our simulations provides evidence to support multistability and hysteresis in this transition, the precise nature of which will be quantified from a Floquet stability analysis in a future study.

The phenomena described above remain qualitatively the same as the length of the filament is changed. However, both the time period and amplitude of the oscillations increase with the filament length, as shown in insets of Figs. 4(a) and 4(b). Remarkably, both these quantities appear to obey a scaling relation $L^{-\alpha} f(\mathcal{A}/L^\beta)$, as shown in the main panels. We estimate the exponents to be $\alpha = -\beta = 1.3$ for the time period and $\alpha = -1.5, \beta = -1.3$ for the amplitude.

To better understand the role of hydrodynamic interactions, we have performed a linear stability analysis on the free-draining continuum limit of this model. Our results, obtained analytically, show that the spectrum of the clamped filament system in this limit is purely real,

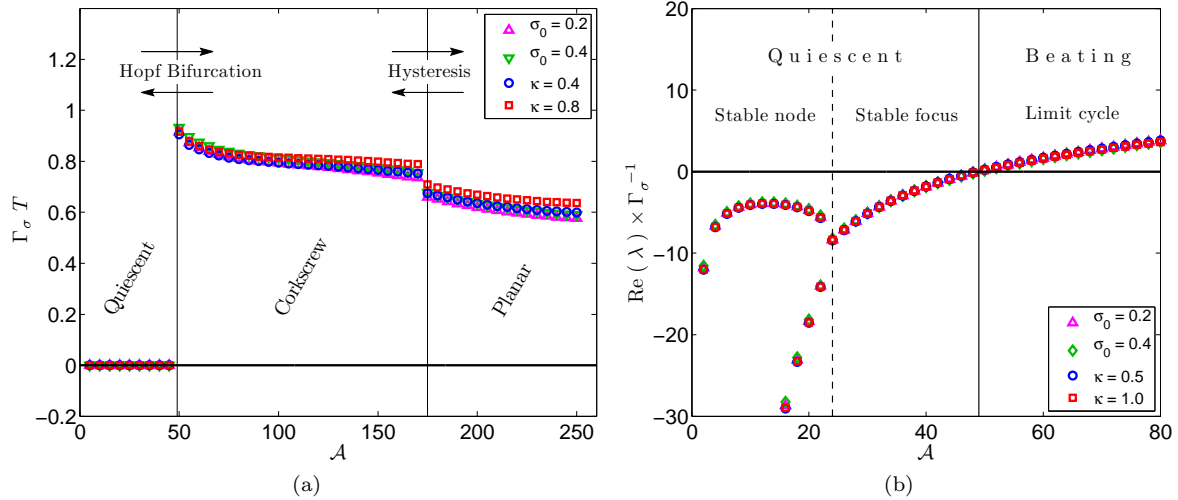


FIG. 3. (Color online) Variation of (a) the scaled timeperiod of filament beating and (b) the real parts of its primary eigenvalues with the activity number \mathcal{A} , plotted for various values of κ and σ_0 . In (a) we show the appearance of spontaneous oscillations in the filament at $\mathcal{A} \sim 50$ corresponding to rigid corkscrew rotation, followed by a transition at $\mathcal{A} \sim 180$ to flexible planar beating. In (b) we demarcate the various dynamical regimes of the filament obtained from linear stability analysis. The collapse of the different plots onto a single master curve for both (a) and (b) shows that \mathcal{A} completely determines filament dynamics at fixed L .

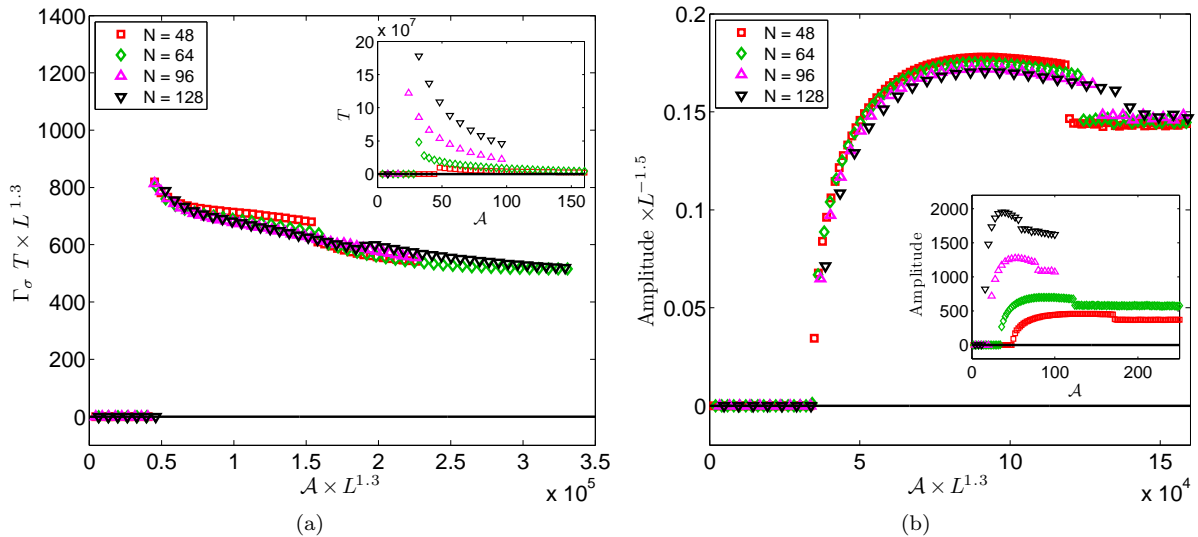


FIG. 4. (Color online) Variation of the rescaled (a) timeperiod and (b) amplitude of filament beating with the length L and activity number \mathcal{A} . The unscaled results in the insets show that the time period as well as the amplitude of beating increases with L , while the rescaled main panels show that these variations are well captured by a scaling form $L^{-\alpha} f(\mathcal{A}/L^\beta)$. Our estimates are $\alpha = -\beta = 1.3$ for the time period and $\alpha = -1.5, \beta = -1.3$ for the amplitude.

with the transition to instability occurring via a saddle-node bifurcation, as seen in Fig. (5). This rules out any oscillatory modes of the filament. Since the free-draining approximation only takes local hydrodynamics into account, this analysis suggests that hydrodynamic interactions are required to produce an oscillatory instability in our model active filament.

It is thus quite extraordinary that this minimal

nonequilibrium active filament model shows spontaneous emergent biomimetic behavior which is reminiscent of the rhythmic oscillations of various prokaryotic and eukaryotic flagella [20–27]. The generic nature of our model indicates that chains of elements which convert chemical energy to mechanical stresses in a fluid environment, for instance synthetic catalytic nanorods [16–19], should exhibit the behaviour described here. Our results lead us to

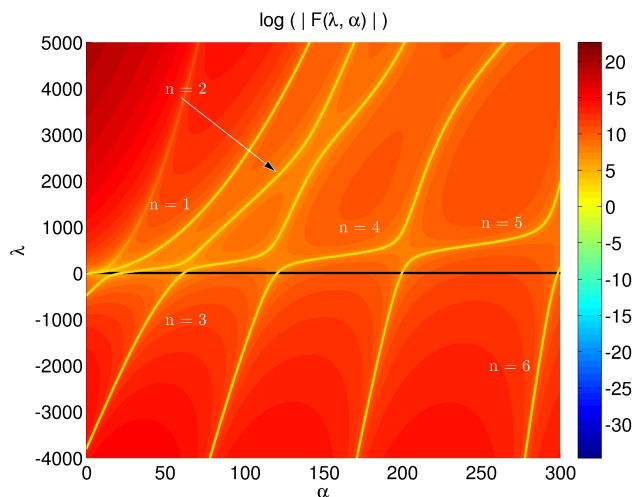


FIG. 5. (Color) Logarithm of the absolute value of the characteristic function F as a function of λ and α , obtained analytically in the free-draining approximation. The golden lines track the zero contours, and correspond to the various normal modes as indicated. The transition to instability occurs via a saddle-node bifurcation.

conclude that hydrodynamic instabilities due to internal active stresses are sufficient ingredients to induce spontaneous biomimetic beating in a clamped active filament.

Financial support from PRISM, Department of Atomic Energy, Government of India and computing resources through HPCE, IIT Madras and Annapurna, IMSc are gratefully acknowledged. We thank M. E. Cates, Z. Dogic, D. Frenkel, G. Baskaran, I. Pagonabarraga, and R. Simon for helpful discussions.

-
- [1] K. E. Machin, *Journal of Experimental Biology* **35**, 796 (1958).
- [2] C. J. Brokaw, *The Journal of experimental biology* **55**, 289 (1971).
- [3] J. Lighthill, *SIAM review*, 161 (1976).
- [4] M. Hines and J. J. Blum, *Biophysical journal* **23**, 41 (1978).
- [5] S. Gueron and N. Liron, *Biophysical journal* **63**, 1045 (1992).
- [6] C. B. Lindemann, *Journal of Theoretical Biology* **168**, 175 (1994).
- [7] S. Camalet, F. Jülicher, and J. Prost, *Phys. Rev. Lett.* **82**, 1590 (1999).
- [8] S. Camalet and F. Jülicher, *New Journal of Physics* **2**, 24 (2000).
- [9] R. Dillon and L. Fauci, *Journal of theoretical biology* **207**, 415 (2000).
- [10] I. H. Riedel-Kruse, A. Hilfinger, J. Howard, and F. Jülicher, *HFSP journal* **1**, 192 (2007).
- [11] N. Kikuchi, A. Ehrlicher, D. Koch, J. A. Käs, S. Ramaswamy, and M. Rao, *Proc. Natl. Acad. Sci.* **106**, 19776 (2009).
- [12] S. E. Spagnolie and E. Lauga, *Physics of Fluids* **22**, 031901 (2010).
- [13] T. Sanchez, D. Welch, D. Nicastro, and Z. Dogic, *Science* **333**, 456 (2011).
- [14] T. Sanchez, D. Chen, S. DeCamp, M. Heymann, and Z. Dogic, *Nature* **491**, 431 (2012).
- [15] G. Jayaraman, S. Ramachandran, S. Ghose, A. Laskar, M. Saad Bhamla, P. B. Sunil Kumar, and R. Adhikari, *Physical Review Letters* **109**, 158302 (2012).
- [16] W. F. Paxton, K. C. Kistler, C. C. Olmeda, A. Sen, S. K. S. Angelo, Y. Cao, T. E. Mallouk, P. E. Lammert, and V. H. Crespi, *J. Am. Chem. Soc.* **126**, 13424 (2004).
- [17] J. Vicario, R. Eelkema, W. R. Browne, A. Meetsma, R. M. La Crois, and B. L. Feringa, *Chem. Commun.* **31**, 3936 (2005).
- [18] G. A. Ozin, I. Manners, S. Fournier-Bidoz, and A. Arsenault, *Adv. Mater.* **17**, 3011 (2005).
- [19] J. M. Catchmark, S. Subramanian, and A. Sen, *Small* **1**, 202 (2005).
- [20] T. L. Jahn and E. C. Bovee, *Annual review of microbiology* **19**, 21 (1965).
- [21] J. Gray, *Journal of Experimental Biology* **32**, 775 (1955).
- [22] C. B. Lindemann and R. Rikmenspoel, *Science* **175**, 337 (1972).
- [23] H. C. Berg and R. A. Anderson, *Nature* **245**, 380 (1973).
- [24] H. Berg, *Biochemistry* **72**, 19 (2003).
- [25] E. Purcell, *Am. J. Phys* **45**, 3 (1977).
- [26] C. Brokaw, *Journal of Experimental Biology* **43**, 155 (1965).
- [27] C. J. Brokaw, *The Journal of cell biology* **114**, 1201 (1991).
- [28] M. Fujimura and M. Okuno, *The Journal of experimental biology* **209**, 1336 (2006).
- [29] J. Blake, *J. Fluid Mech* **46**, 199 (1971).
- [30] C. Brennen and H. Winet, *Annual Review of Fluid Mechanics* **9**, 339 (1977).
- [31] E. Lauga and T. Powers, *Reports on Progress in Physics* **72**, 096601 (2009).
- [32] S. Ramaswamy, *Annual Review of Condensed Matter Physics* **1**, 323 (2010).
- [33] M. Cates and F. MacKintosh, *Soft Matter* **7**, 3050 (2011).
- [34] M. C. Marchetti, J.-F. Joanny, S. Ramaswamy, T. B.

Liverpool, J. Prost, M. Rao, and R. Aditi Simha, ArXiv e-prints (2012), [arXiv:1207.2929 \[cond-mat.soft\]](#).